

Document downloaded from:

<http://hdl.handle.net/10251/142278>

This paper must be cited as:

Teixeria, R.; Santos, S.; Christoforo, A.; Paya Bernabeu, JJ.; Savastano Jr., H.; Rocco Lhar, F. (09-2). Impact of content and length of curauá fibers on mechanical behavior of extruded cementitious composites: Analysis of variance. *Cement and Concrete Composites*. 102:134-144. <https://doi.org/10.1016/j.cemconcomp.2019.04.022>



The final publication is available at

<https://doi.org/10.1016/j.cemconcomp.2019.04.022>

Copyright Elsevier

Additional Information

1 **Analysis of variance: content and length of curauá fibers on mechanical**
2 **behavior of extruded cementitious composites**

3
4 R.S. Teixeira ^{a*}, S.F. Santos ^b, A.L. Christoforo ^c J.B. Paya ^d, H. Savastano Jr. ^e, F.A.
5 Rocco Lahr ^a

6
7 ^a *University of São Paulo, Department of Structural Engineering, Av. Trabalhador São Carlense,*
8 *400, 13566-590, São Carlos/SP, Brazil, e-mail: ronaldostx@yahoo.com.br;*

9 ^b *São Paulo State University, Department of Materials and Technology, Av. Ariberto Pereira da*
10 *Cunha, 333, 12516-410, Guaratingueta/SP, Brazil;*

11 ^c *Federal University of São Carlos, Department of Civil Engineering, Rodovia Washington Luís,*
12 *Km 235, s/n, 13565-905, São Carlos/SP, Brazil;*

13 ^d *Polytechnic University of Valencia, Institute of Science and Concrete Technology, Camino de*
14 *Vera s/n, Edificio 4N, E-46022, Valencia, Spain;*

15 ^e *University of São Paulo, Department of Biosystems Engineering, Av. Duque de Caxias Norte, 225,*
16 *13635-900, Pirassununga/SP, Brazil.*

17 **Corresponding member*

18

19 **ABSTRACT**

20 The use of composite materials in construction has grown considerably in recent years, such as
21 cementitious matrices and concrete reinforced with fibers. The vegetable fibers have become an
22 alternative due to its abundance, low cost and low energy consumption for its production, and
23 appropriate properties mechanical. Curauá fiber is a plant native from Amazonas harvested
24 manually in commercial farming and it is used in the manufacture of ropes and baskets or as
25 reinforcement in composite with organic matrix of components for cars, buses and trucks. On
26 the other hand, the extrusion process can produce composites with high-density matrix with
27 fibers, low permeability and good interface between fiber and matrix. This process is also
28 compatible with the use of vegetable fibers as raw materials in the production of cost-effective
29 construction elements such as ceiling panels and drywalls. The objective of this research was
30 use the analysis of variance (ANOVA) for evaluating the content and length of curauá fibers on
31 the mechanical behavior of the extruded cementitious composites. Composites without fibers
32 and reinforced with 1% and 2% by mass of fibers as well as 6 mm and 10 mm of length these
33 curauá fibers were evaluated. The composites with fibers of 10 mm have showed better
34 mechanical results. Besides, the composites with fibers curauá after 200 accelerated aging
35 cycles were better than one non-aging.

36 **Keywords: Mechanical of fracture; extrusion process; lignocellulosic fiber; Amazonian fiber.**

* Corresponding author. E-mail address: ronaldostx@yahoo.com.br and ronaldost@usp.br (R.S. Teixeira). Tel.: +55 19 3565 4269;

1. INTRODUCTION

Fiber-cement products had been widely used in the world due to their versatility as corrugated and flat roofing materials, cladding panels, and water containers presented in large number of building and agriculture applications [1,2].

In order to improve the sustainability of construction materials, part of the global strategy is to use regional, recyclable and renewable materials from agroindustrial resource and environmentally appropriate technologies for civil construction. Recent years new technologies using lignocellulosic fiber have arisen enabling the use of composites with less environmental impact, low cost and low power consumption, allowing replace partially synthetic fibers, such as polypropylene or polyvinyl alcohol [1,3–5].

The incorporation of lignocellulosic fibers mostly co-product of agriculture and agro-industries, allows a valorization of these residues and a limitation of environmental damages [1,6].

The curauá fiber is a plant native from Amazon and a hydrophilus species belongs to pineapple/bromeliad family. It is a lignocellulosic fiber that has mechanical properties comparable to synthetic polymeric fiber [7–10].

As part of the global strategy to produce regional and environmental-friendly materials the extrusion technology has been successfully as an economical, efficient and processing method for manufacturing sustainable fiber-reinforced cement based composites [11,12]. Other advantage of the extrusion process is its capacity of producing not only flat shapes, but also structural and complex shapes. Besides, this process allows the use of a variety of materials that have been successfully incorporated such as lignocellulosic fiber, including, sugar cane fiber [4] and sisal fiber [13].

However, It is known the problem of reduction of lignocellulosic fiber durability caused mainly by the alkaline (pH around 12) environment of the cement matrix and, consequently causing a destruction of the macromolecular chains during the partial alkaline hydrolysis, initially the lignin after that the cellulose, which decrease of the degree of polymerization of the both phases [14–16].

Other mechanism is the gradual filling of the inner cores of the lignocellulosic fibers with the cement hydration products, leading to the embrittlement of the fibers. These mechanisms could affect some important properties of the reinforced composites, such as toughness mechanisms and other mechanical properties of the fiber-cement in the long-term. [1,17].

The degradation of the composite can be studied by accelerated tests, whose advantage is to provide results in a smaller time interval [18,19]. The durability test (accelerating aging) of the cementitious

69 composites shows their performance in the presence of wet/dry cycling and therefore may be
70 recommended for both internal and external building applications [16,20].

71 In this study was evaluated statically, with analysis of variance (ANOVA), mechanical behavior of
72 extruded fiber-cement composites reinforced with curauá fiber with different content and lengths,
73 before and after accelerated aging.

74

75 **2. EXPERIMENTAL**

76 **2.1. Raw materials**

77 Curauá fibers (CF) (*Ananas erectifolius*) used in this study was obtained from the Pematec Triangel
78 Industry in Pará/PA, Brazil. Mechanical and physical properties and chemical composition of the
79 fiber are listed in Table 1.

80

81 Table 1 – Mechanical, chemical and physical properties of the curauá fiber

	Curauá fiber (CF)
Ultimate tensile strength (MPa)	550
Young's modulus (GPa)	64
α -Cellulose ¹ (% by mass)	68
Lignin ² (% by mass)	14
Hemicellulose ³ (% by mass)	10
Average length (mm)	6.00 ± 0.88 and 10.00 ± 0.46
Cross section (mm ²)	0.1136
Thickness (μm)	~75
Density (g/cm ³)	1.42
Aspect Ratio	~80 and ~133

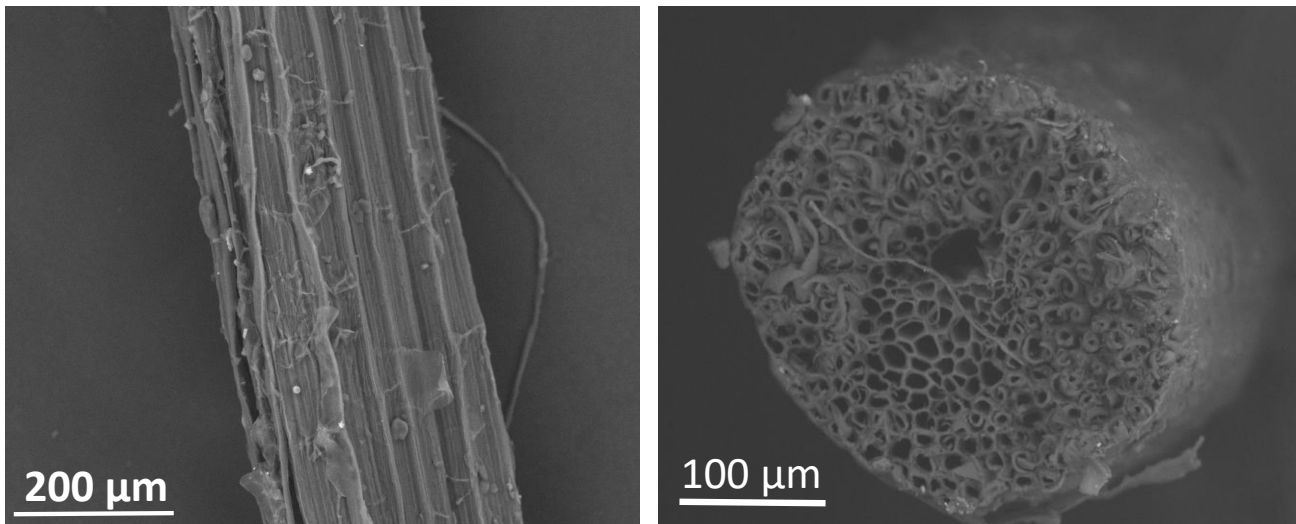
82 1 TAPPI T 204 CM-97 [21]; 2 Zimmermann et al., [22]; 3 TAPPI T 222 OM-02 [23].

83

84 The results of the chemical composition of the curauá fibers were similar found in the literature. For
85 example, It was found a range between 73% by mass and 71% by mass of cellulose and 7.5% by
86 mass to 13% by mass of lignin [24,25]. It is important to consider that there is a natural variation in
87 the analysis of chemical composition of vegetable fibers by means of quantification methods and
88 characteristics of the fibers of a specific region and harvested at different times throughout the
89 season.

90 Figure 1a shows a surface roughness of the curauá fiber and Figure 1b shows its cross section,
91 approximately elliptical shape. These characteristics help to anchor better in cementitious matrix.
92 Besides, in Figure 1b, it is possible to observe unit cells and lumens (cavities) of the fiber cross
93 section.

94



(a)

(b)

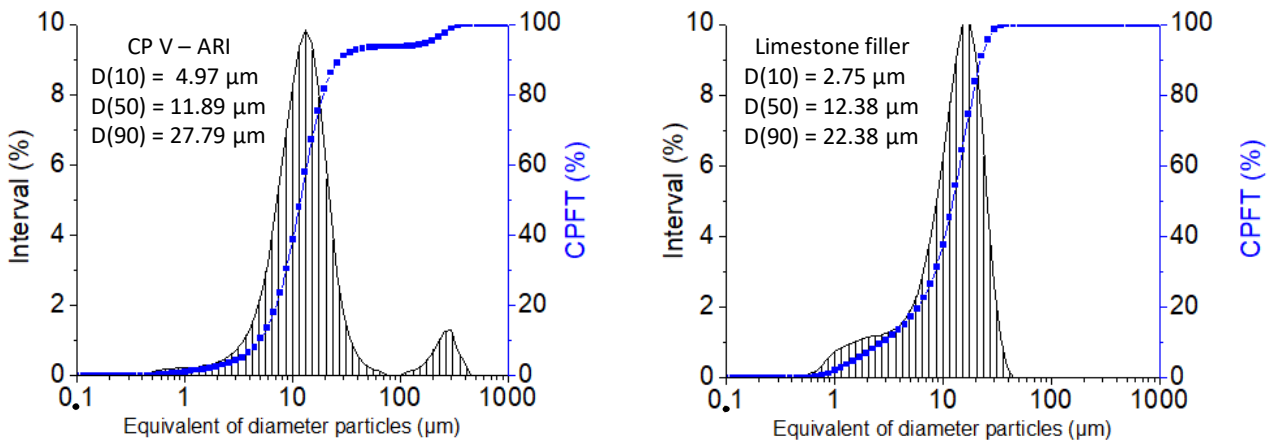
Figure 1 – Morphological characteristics of CF observed by scanning electron microscopy. (a) Lateral surface and (b) cross-section detaching the irregular lumens [26].

95

96 Unbleached unrefined eucalyptus (*Eucalyptus grandis*) Kraft pulp was provided by Fibria S/A,
97 Brazil. The cellulose pulp was collected directly from the mill, prior to drying and pressing. It was
98 extensively washed with water and centrifuged to remove any residual chemicals from the pulping
99 processes.

100 Ordinary Portland cement (OPC) type CP-V-ARI, corresponding to ASTM C 150 [27], Type I was
101 selected because of its finer particle size and higher reactivity. Additionally, this type of cement
102 contains higher levels of tricalcium silicate (C_3S) and dicalcium silicate (C_2S) for the formation of
103 C–S–H. The cement and limestone filler particles distributions were evaluated by a laser particle
104 size analyzer (Malvern Mastersizer S long bed, version 2.19). The particle size distributions of the
105 raw materials are depicted in Figure 2. Figures 2a and 2b show the discrete particle size
106 distributions and the cumulative percentage finer than (CPFT) of the cement and limestone filler,
107 respectively. Cement and limestone particles showed 50% of its mass less than 11.89 and 12.38 μm ,
108 respectively. Both raw materials exhibit similar particle distributions.

109



(a)

(b)

Figure 2 – (a) Particle size distribution of ordinary Portland cement and (b) limestone filler. The legend indicates the maximum equivalent diameter for each accumulated percentage of particles

110

111 The quantitative chemical analysis was performed of the OPC and limestone using PANalytical
 112 Axios Advanced X-ray fluorescence equipment. The oxides are listed in Table 2. The specific
 113 surface area (determined using the BET method) and specific density of raw materials were
 114 measured. The OPC presented value of specific density of 3.10 g/cm^3 and specific surface area of
 115 $1.10 \text{ m}^2\text{g}^{-1}$ and for limestone 2.80 g/cm^3 and $1.14 \text{ m}^2\text{g}^{-1}$, respectively. The similar values of the
 116 specific surface area may be important to avoid competition of water between the raw materials in
 117 the system.

118

119 Table 2 – Chemical analysis by means of X-ray fluorescence of the particulate raw materials (% by
 120 mass).

Oxides compositions	Ordinal Portland cement (OPC) CP-V-ARI	Limestone
SiO ₂ (%)	14.70	9.40
CaO (%)	67.20	39.10
Al ₂ O ₃ (%)	4.07	2.16
Fe ₂ O ₃ (%)	3.50	1.25
MgO (%)	3.13	8.90
P ₂ O ₅ (%)	-	0.16
SO ₃ (%)	5.23	-
K ₂ O (%)	0.75	0.41
MnO (%)	-	<0.10
TiO ₂ (%)	-	0.15

121

122 **2.2. Formulation and preparation of composites cementitious**

123 The composite is composed of CP-V-ARI cement and limestone filler. The water-soluble polymers,
 124 high range water reducer (HRWR) provided by Aditex and polyether carboxylic provided by Grace
 125 was used as lubricant, representing 1% of cement mass. Hydroxypropylmethylcellulose (HPMC)

126 with an average molecular weight of 86,000 and a viscosity of 5.39 cps (at a concentration of 2% in
 127 water at 20 °C) and carboxylate polyether (surfactant) commercially called ADVA 170, were used
 128 as rheological modifiers to promote pseudo plastic behavior of the composite. As curauá fibers
 129 present higher real density (1.42 g/cm³), the fiber contents were set in relation to polypropylene
 130 fibers (0.92 g/cm³) to maintain the same volume reinforcement. The mix design used in this work is
 131 in Table 3.

132
 133 Table 3 – Formulations used in the production of cementitious composite

Raw material	Content [% by mass] / length				
	Ref	1% / 6 mm	2% / 6 mm	1% / 10 mm	2% / 10 mm
Portland cement [CP-V-ARI] ^a	69.95	68.87	67.79	68.87	67.79
Limestone filler ^b	27.08	26.66	26.54	26.66	26.54
Eucalyptus cellulosic pulp	2.98	2.93	2.89	2.93	2.89
Curauá fiber (CF)	-	1.53	3.08	1.53	3.08
Water/cement ratio	0.33	0.34	0.36	0.34	0.36

134 (a) ASTM C-150 [27]; (b) Provided by Infibra Ltda; (c) volume fraction of fibers in study: 3% and 6%,
 135 respectively.

136
 137 The sequence of mixing was powder/water [28]. The cement, limestone, curauá fiber (CF) and
 138 HRWR (by dry mass) were mixed and homogenized at low speed (mixture distributive), in a
 139 mechanical Eirich intensive mixer (capacity of 10 L) for 5 min. After this stage, water and
 140 carboxylate polyether was added fractionally for 2 min. All raw materials was mixed at high speed
 141 for another 5 min. to achieve a high shear mixing to break down the agglomeration generated in wet
 142 mixing stage. Before composites production, the composite was re-homogenized in the extruder
 143 itself, feeding it and taking two times the mass.

144 Composites with 15 mm thick were extruded, according to Figures 3a and 3b. An extrusion helical
 145 screw equipment (Auger type), Verdes, model 051, was used. The equipment contains a motor
 146 speed regulator that was maintained by 4 mm/s during extrusion. Pads with 200 mm x 50 mm x 15
 147 mm were cured at water vapor saturated environment (in sealed plastic bags) at 25 ± 2 °C for two
 148 days. Subsequently, the specimens were maintained in a water vapor saturated environment (in
 149 sealed plastic bags) and placed in a chamber at 45 °C for five days (thermal curing) totalizing 7 days
 150 of cure [13].

151



(a) (b)
Figure 3 – (a) Front view of the vacuum extruder machine and (b) side view illustrating the composite exiting of the die [29].

152

153 **2.3. Mechanical characterization of the composites**

154 Mechanical characterization tests were adopted according to Santos et al., [13]. The fiber-
 155 cement composites were tested using a servo-hydraulic mechanical testing machine MTS (810
 156 series) controlled by the TestStar IIs system. Prismatic specimens were prepared using a diamond
 157 cut-off wheel before grinding and final polishing of the specimen sides. The specimens had nominal
 158 dimensions of 80 mm x 20 mm x 13 mm for all of the mechanical tests of the fiber-cement
 159 composite. The modulus of rupture (MOR) was calculated by equation 1 and determined using a
 160 three point bending configuration with a span of 64 mm and cross-head speed of 5 mm min⁻¹.

161

$$162 \text{ MOR} = \left(\frac{3 * P_{\max} * L_V}{2 * b * h^2} \right) \quad (1)$$

162

163 where P_{\max} is maximum load, b is width, h is height and L_V is span between inferior supports.
 164 The fracture toughness (K_{IC}) is the critical stress intensity fracture value for crack growth in the
 165 material during mode-I failure, which evaluates the initial crack growth resistance, was also used to
 166 characterize the cement based composites reinforced with curauá fiber. The SENB-type (single-
 167 edge notch bend) specimens were prepared to establish the critical defect size and catastrophic
 168 fracture [1]. The test configuration was the three-point bending. Prismatic specimens were prepared
 169 with a centered plan notch with a depth equal to 10 % of the specimen height and notch tip profile
 170 in the shape of a “V” with an angle of approximately 30° using a diamond disk of 0.5 mm
 171 thickness to simulate a sharp crack. A cross-head speed of 15 mm min⁻¹ was used. The values of the
 172 maximum load, P_{\max} , from the load–displacement curves were applied in the calculation of the
 173 value of K_{IC} using the following equation, according to Santos et al., [13]:

174

$$K_{IC} = \frac{P_{max}}{bw^{1/2}} y(\alpha) \quad (2)$$

175

176 where $y(\alpha)$ is the geometric factor and accounts for both shape of crack and loading geometry, the
 177 tensile stress at fracture, and a_0 the crack size. The ratio $\alpha = a_0/w$ of the initial notch length to
 178 specimen height was 0.1 (or 10% as mentioned before).

179

$$y(\alpha) = \frac{S}{w} \left[\frac{3\alpha^{1/2}}{2(1-\alpha)^{3/2}} \right] x \left[1.99 - 1.33\alpha - (3.49 - 0.68\alpha + 1.35\alpha^2) \frac{\alpha(1-\alpha)}{(1+\alpha)^2} \right] \quad (3)$$

180

181 where S is the span of 64 mm, and α is the relative length of the notch, which, in turn, is the ratio of
 182 the original length of the notch, a_0 , and the height of the specimen, w .

183 The fracture energy (FE) test was performed with the SENB type specimen and three-point bending
 184 configuration, but the centered plan notch was of 30% of the specimen height. The span was of
 185 64 mm. A cross-head speed of $10 \mu\text{m min}^{-1}$ was used to guarantee stable growth of the crack and to
 186 measure the energy required for extending this crack over a unit area [30].

187 The work performed by the machine to completely propagate the crack along the specimen divided
 188 by two times the projected area of the fracture surface (cross section of the specimen, A) was used
 189 to determine the fracture energy, γ_{Wof} . The integration of the force–displacement curve was
 190 performed up to the point where the force decreased to 5% of its maximum value reached during
 191 the test, according to equation 4:

192

$$\gamma_{Wof} = \frac{1}{2A} \int P d\delta \quad (4)$$

194

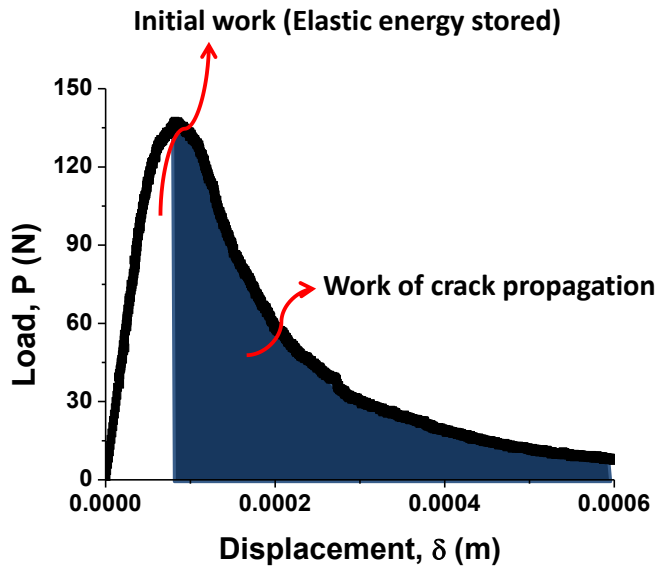


Figure 4 – Schematic illustration of a typical load–displacement curve divided into two regions: initial work and work of crack propagation [13].

195

196 Additionally, a mechanical parameter was obtained the “relative work of crack-propagation” [31].
 197 This mechanical parameter is obtained by dividing the work of crack propagation by the initial
 198 work (elastic energy stored). The initial work is that performed from zero up to the point of the
 199 maximum load (Figure 4). Although up to this point, some crack propagation could already occur, it
 200 is easy to determine. This ratio considers all of the work performed for the effective crack
 201 propagation related to the elastic energy stored in the system. Therefore, a higher value of this
 202 relative work indicates that the material is more resistant to propagation of a crack [31].

203

204 **2.4. Physical characterization tests**

205 Water absorption (WA) apparent porosity (AP) and bulk density (BD) values were obtained from
 206 the average of five specimens for each formulation, following procedures specified by ASTM C
 207 948 [32], Standards.

208

209 **2.5. Scanning electron microscopy (SEM)**

210 Scanning electron microscopy (SEM) was used with secondary electron (SE) detector, operated at
 211 5.0 kV accelerating voltage, for observation of the morphologies on the fractured surface of
 212 composites generated in the mechanical tests. A back-scattered electron (BSE) detector operated at
 213 around 15.0 kV and 20.0 kV was applied for viewing cut and polished surfaces. The BSE image
 214 was used to study the fiber–matrix transition zone. Energy dispersive X-ray spectroscopy (EDS)
 215 analyses were also conducted. These were performed on the same flat surface specimens in an effort

216 to obtain semi-quantitative compositional information. The preparation of specimens for BSE and
 217 EDS was accomplished with vacuum (80 kPa gauge) impregnation using cyanoacrylate ester resin.
 218 BSE EDS samples were semi-automatic grinded with silicon carbide abrasive paper with sequential
 219 grit sizes of 320, 600, 1200 and 2000 for 2 min each, using alcohol as lubricant. A final preparation
 220 was carried out using in turn 8–4 , 4–2 and 1–0 μm diamond polishing compound during 4, 2 and 1
 221 min each size respectively. Fractured and polished samples were gold coated in a Bal-Tec Med020
 222 coating system before being analyzed in a Hitachi TM 3000 microscope.

223

224 **2.6. Accelerated aging testing**

225 The accelerated aging testing involved a comparative analysis of physical and mechanical
 226 performance of the composites, before and after 200 soak/dry cycles. Specimens were successively
 227 immersed in water at 20 ± 5 °C during 170 min, followed by the interval of 10 min, and then
 228 exposed to temperature of 70 ± 5 °C for 170 min in a ventilated oven and with the final interval of
 229 10 min. This procedure was based on recommendations of the EN 494 [33], Standards. Each
 230 soak/dry set represents one cycle and was performed for 200 cycles (200C) [4].

231

232 **2.7. Statistical analysis**

233 The physical and mechanical properties evaluated were: water absorption (WA), apparent porosity
 234 (AP), apparent density (BD), modulus of rupture (MOR), fracture energy (FE), fracture toughness
 235 (K_{IC}) and relative work of crack propagation (RWP). The factors and levels investigated consisted
 236 of curauá fiber fractions (% F) [1, 2%], fiber length (FL) [6, 10 mm] and curing type (Cr) [7d (0),
 237 200C (1)]. The product of the three factor levels along with the reference conditions [Ref] (0% fiber
 238 and 7 days cure [Tr1], 0% fiber resulted in an experimental design consisting of 9 treatments, as
 239 explained in Table 4. It should be noted that the treatment Tr1 (reference) was used in the
 240 manufacture of materials for the determination of physical and mechanical properties.

241

242 Table 4 – Experimental treatments.

Formulation	Treatment (Tr)	%F	FL	Cr
Ref	Tr1	0	0	7 days (0)
1% / 6 mm	Tr2	1%	6 mm	7 days (0)
1% / 10 mm	Tr3	1%	10 mm	7 days (0)
2% / 6 mm	Tr4	2%	6 mm	7 days (0)
2% / 10 mm	Tr5	2%	10 mm	7 days (0)
1% / 6 mm	Tr6	1%	6 mm	200C (1)
1% / 10 mm	Tr7	1%	10 mm	200C (1)
2% / 6 mm	Tr8	2%	6 mm	200C (1)
2% / 10 mm	Tr9	2%	10 mm	200C (1)

243 The methodology of Experimental Planning (DOE), using Minitab® software version 14, was used
244 to establish the relationship between the properties (physical and mechanical) and the factors
245 evaluated, to understand the effects and to identify the factors and interactions considered
246 significant and to identify the treatments that resulted in the extreme values of the properties
247 estimated by the models. The analysis of variance (ANOVA) of regression models (Equation 5) was
248 evaluated at the 5% level of significance (α), considering the non-significance (P-value <0.05) of
249 the models and coefficients as null hypothesis (H0) and significance as an alternative hypothesis
250 (H1). For the validation of the regression models, the normality of the generated residues was tested
251 with the aid of the Anderson-Darling normality test, also at the 5% level of significance, and for the
252 hypotheses formulated, P-value greater than or equal to 0.05 implies in the normality of the waste
253 distribution, validating the ANOVA model.

254

$$Y = \beta_0 + \beta_1 \cdot \%F + \beta_2 \cdot FL + \beta_3 \cdot Cr + \beta_4 \cdot \%F \cdot FL + \beta_5 \cdot \%F \cdot Cr + \beta_6 \cdot FL \cdot Cr + \beta_7 \cdot \%F \cdot FL \cdot Cr + \varepsilon \quad (5)$$

255

256 From Equation 5, Y denotes the estimated physical and mechanical properties, β_i are the
257 coefficients obtained from the least squares method and ε consists of the random error. The
258 coefficient of determination (R^2) was used to measure the quality of the adjustments obtained, and it
259 should be noted that the reference conditions are not incorporated in the regression models.
260 In planning involving the 9 treatments after understood the effects of factors and interactions
261 between them on each property investigated. It can be noted that 6 or more determinations were
262 obtained by treatment and property investigated, totaling 382 determinations.

263

264 **3. RESULTS AND DISCUSSION**

265

265 ***3.1. Mechanical properties***

266 Figure 5 shows the mechanical properties (modulus of rupture (MOR), fracture toughness (K_{IC}),
267 fracture energy (FE), and relative work of crack propagation (RWP)) of extruded cementitious
268 composite (ECC) cured at 7 days (7d), after accelerated aging (200C), the confidence intervals of
269 the mean (at the 95% confidence level) and the range of variation of the coefficient of variation
270 (CV). Table 5 lists the respective average values and standard deviations of the mechanical
271 properties and physical characteristics. The P-values of the Anderson-Darling normality test of the
272 ANOVA residues for the four mechanical properties (MOR, K_{IC} , FE and RWP, respectively)
273 evaluated ranged from 0.265 to 0.781, validating the ANOVA model, and by the results of the
274 determination coefficients [79.72%; 99.02%], it is verified the good estimation of the properties

275 provided by the models, being all considered significant by ANOVA. Equations 6 and 7 expresses
276 the regression model obtained in the estimation of the MOR and K_{IC} values, respectively, and also
277 the coefficients of determination (R^2) and the numerical intervals of this property are presented.
278 Equations 6 and 7, the outliers were excluded from the set of results, and the terms considered non-
279 significant by ANOVA of the regression models were underlined.
280

$$\text{MOR} = 1.39775 + 9.30425 \cdot \%F + 1.55238 \cdot \underline{\text{FL}} + 20.7527 \cdot \text{Cr} - 1.05938 \cdot \%F \cdot \text{FL} - 14.2959 \cdot \%F \cdot \text{Cr} \\ 1.23217 \cdot \text{FL} \cdot \text{Cr} + 1.14854 \cdot \%F \cdot \text{FL} \cdot \text{Cr} \quad (R^2 = 79.72\%); \text{MOR} = [12.19; 23.18] \quad (6)$$

$$K_{IC} = 0.878467 - 0.0865817 \cdot \%F - 0.0040055 \cdot \text{FL} + 0.438194 \cdot \text{Cr} + 0.0117967 \cdot \%F \cdot \text{FL} \\ 0.332244 \cdot \%F \cdot \text{Cr} - 0.0522791 \cdot \underline{\text{FL}} \cdot \text{Cr} + 0.0312871 \cdot \%F \cdot \text{FL} \cdot \text{Cr} \quad (R^2 = 81.65\%); K_{IC} = [0.64; 1.08] \quad (7)$$

281
282 ECC reinforced with 2% of curauá fiber (CF) at 7d showed a significant increase of MOR values in
283 relation to the ECC with 1% of CF and reference (Ref), according the ANOVA test shown in
284 Equation 6 and Figure 5a. However, the results of fiber length did not differ significantly between
285 the formulations. The MOR is the tensile strength in bending as well as it is influenced by
286 interaction and distribution of stresses between fiber-matrix and matrix porosity. The inclusion of
287 fibers increases the toughness and the reinforcement of composites, but also increases the porosity
288 because the dispersion deficiency of the fibers in cementitious matrix and, consequently, generating
289 lack of stress transfer between the fibers and matrix. After 200C, Figure 5a, the MOR values of the
290 ECC increased due to the combined effect better adhesion (increase in chemical bonding) of CF in
291 the cementitious matrix, the continued hydration process in the fiber-matrix interface and
292 petrification or mineralization these fibers [34].

293 According Melo Filho et al., [17], the mineralization occurs under conditions in which the cement
294 hydration products migrate to the more porous regions within the fibers (surface pores and lumens).
295 From the interaction between the three statistical factors (fiber fractions (% F) [1, 2%], fiber length
296 (FL) [6, 10 mm] and curing type (Cr) [7d, 200C]), the highest value occurs from the combination
297 with 2% of fibers, 10 mm in length and after 200C.

298 MOR values found in this study are around 16 MPa to 7d and 20 MPa after 200C for the
299 formulation 1% / 10 mm. These MOR values were higher than those found in previous studies with
300 ECC reinforced with sisal and sugarcane fibers, with respective content of 1% by mass and 1.5% by
301 mass and the distribution of lengths between 15 mm to 18 mm and 10 mm to 15 mm that showed,
302 respectively, MOR values of 8 MPa to 11 MPa for 28 days (28d) and 4 MPa to 15 MPa after 200C
303 [4,35].

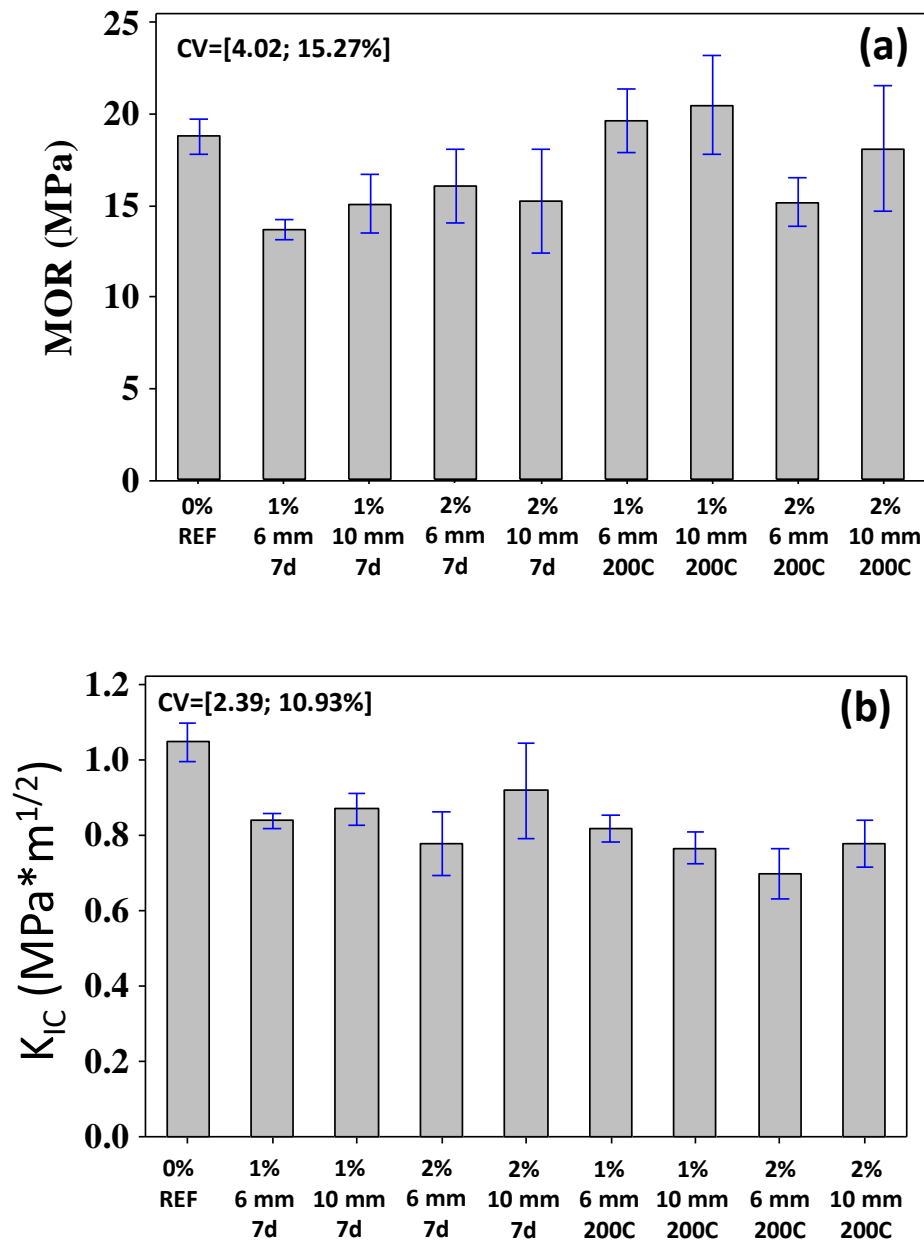


Figure 5 – Average values and standard deviation (MOR) modulus of rupture (a) and (K_{IC}) fracture toughness (b).

304

305 The individual statistical interactions as the higher content (%F) and fiber length (FL) decrease K_{IC}
 306 values, i.e., initial crack growth resistance in cement matrix, according to ANOVA, as calculated by
 307 the equation 7 and whose values are shown in Figure 5b. The K_{IC} value of the reference composites
 308 (1.05 MPa·m^{1/2}) suggests that these results may be related to distribution of defects in the matrix
 309 produced by several factors such as the difficulty in packaging fiber in the matrix with particles and
 310 negative interference in cement hydration process caused by absorption of water by CF. However,

311 the statistical combination of 2% by mass of fiber with 10 mm length after 200C increases the K_{IC}
312 values. It indicates that the matrix was improved mainly after 200 cycles of immersion and drying.
313 The results of fracture toughness of the composites reinforced with CF are similar than the results
314 obtained by Santos et al., [13]. The authors produced cement composites, reinforced with 3%
315 eucalyptus pulp and 2% of sisal fibers, produced by the extrusion method and subjected to
316 accelerated carbonation curing in the supercritical condition. The authors also analyzed the
317 composite before and after 200 cycles of immersion and drying. The average results obtained was
318 $0.9 \text{ MPa}\cdot\text{m}^{1/2}$ and $0.85 \text{ MPa}\cdot\text{m}^{1/2}$, for the unaged and aged composites, respectively.

319 Table 5 – Average values and standard deviations of modulus rupture (MOR), fracture toughness (K_{IC}), fracture energy (FE), relative work of
 320 propagation (RWP), water absorption (WA), bulk density (BD) and apparent porosity (AP) of the extruded cementitious composite (ECC) reinforced
 321 with curauá fiber (CF), 6 mm and 10 mm of length in the conditions at 7 days (7d) of curing and after 200 accelerated aging cycles (200C).
 322

Formulations	Condition	MOR (MPa)	K_{IC} (MPa.m ^{1/2})	FE (J/m ²)	RWP	WA (%)	BD (g/cm ³)	AP (%)
Reference (Ref)	7d	18.75 ± 0.75	1.05 ± 0.04	187.61 ± 16.07	9.77 ± 4.22	16.14 ± 0.28	1.702 ± 0.013	27.47 ± 0.34
1% / 6 mm	7d	13.82 ± 0.57	0.83 ± 0.02	108.20 ± 13.58	3.21 ± 0.67	16.49 ± 0.20	1.708 ± 0.007	28.16 ± 0.29
1% / 10 mm		15.85 ± 1.66	0.88 ± 0.03	309.98 ± 15.98	14.65 ± 5.59	17.22 ± 0.15	1.729 ± 0.055	29.78 ± 0.84
2% / 6 mm		16.01 ± 1.92	0.78 ± 0.08	102.05 ± 9.05	3.66 ± 0.80	18.48 ± 0.72	1.726 ± 0.016	31.90 ± 0.96
2% / 10 mm		15.21 ± 2.26	0.92 ± 0.10	245.09 ± 89.49	14.04 ± 3.13	17.04 ± 0.24	1.720 ± 0.031	29.31 ± 0.59
1% / 6 mm	200C	19.52 ± 1.63	0.82 ± 0.03	45.67 ± 4.28	1.41 ± 0.42	16.73 ± 0.14	1.740 ± 0.009	29.10 ± 0.23
1% / 10 mm		20.45 ± 2.17	0.77 ± 0.03	56.75 ± 5.83	1.43 ± 0.63	17.41 ± 0.10	1.754 ± 0.044	30.54 ± 0.72
2% / 6 mm		15.16 ± 1.27	0.70 ± 0.06	20.18 ± 2.51	0.61 ± 0.25	17.77 ± 0.27	1.725 ± 0.008	30.66 ± 0.40
2% / 10 mm		18.08 ± 2.77	0.78 ± 0.05	41.75 ± 3.89	1.67 ± 1.17	17.59 ± 0.19	1.723 ± 0.027	30.31 ± 0.39

323 Figures 6a to 6d shows the micrographs of ECC with polished surface, Ref and reinforced with CF
324 at 7d and 200C respectively, that it showed a homogenous microstructure of the cement matrix at
325 7d and more densified after 200C. The composite reinforced with CF, (Figure 6c and 6d) content
326 high porosity in the fiber-matrix interface, i.e., it has a low adhesion which do not lead to expressive
327 values of MOR and K_{IC} in relation to the Ref. In the mixing process, the ECC with CF consumed
328 more water, which promotes the formation of porosity and interferes strongly in the w/c ratio
329 (water/cement) and the packaging of the raw materials in the matrix.
330 Figure 6d indicates that the vegetable fiber suffer a dimensional variation because it tends to lose
331 water to the system of the cementitious matrix which in turn is submitted to a rehydration process.
332 This dimensional variation process of the fiber promotes detachment of it in the cementitious
333 matrix, consequently, it affects the mechanical behavior of the cement composite [19].
334

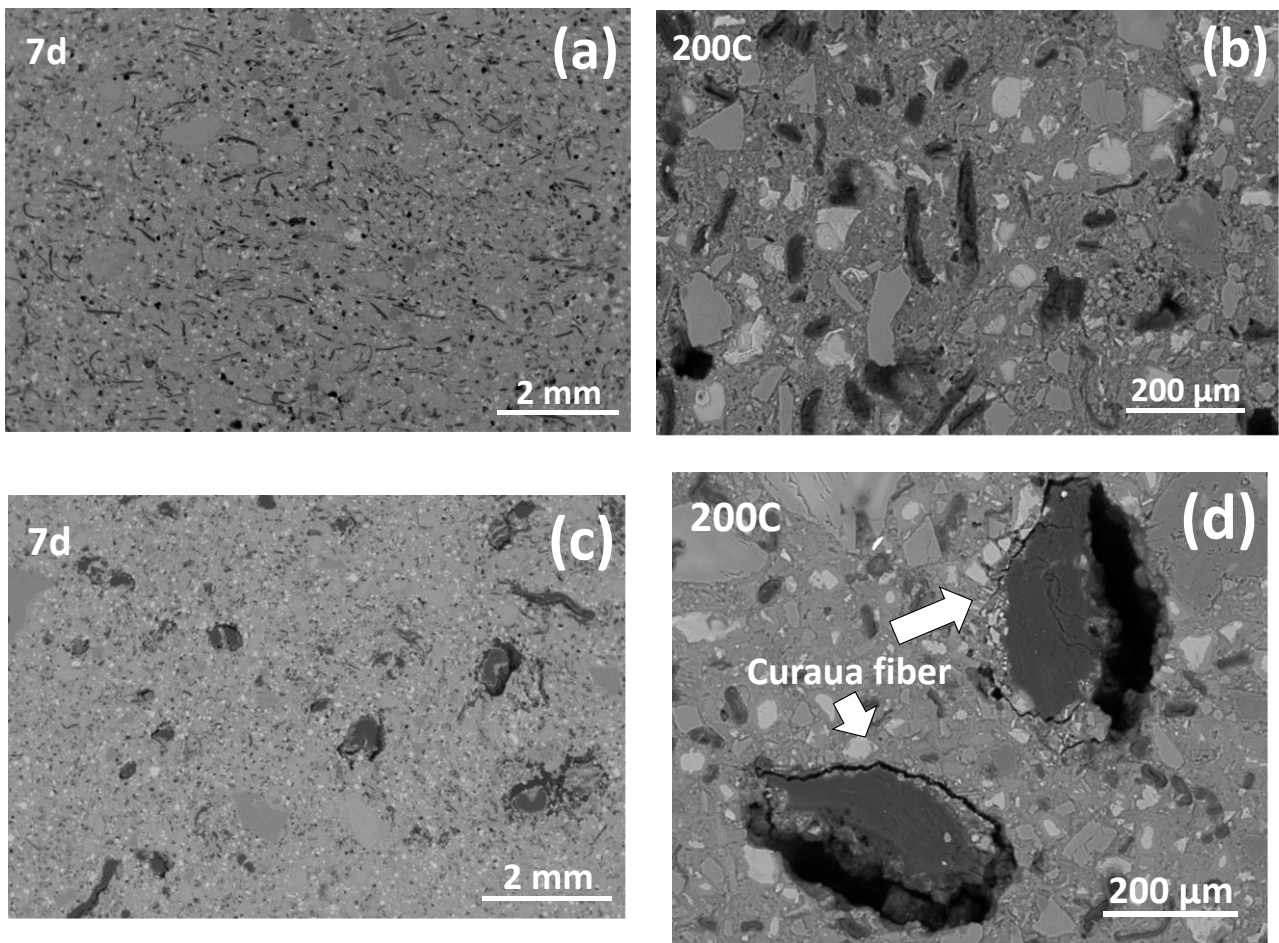


Figure 6 – SEM of the composites at 7d and after 200C, respectively. (a) and (b) reference composite and (c) and (d) composite reinforced with CF.

336 The average values of fracture energy values (FE) and relative working crack propagation (RWP) of
 337 the composite at 7d and after 200C are shown in Figures 7a and 7b, respectively. Equations 8 and 9
 338 expresses the regression analysis obtained in the estimation of the FE and RWP values, and the
 339 coefficients of determination (R^2) and the numerical intervals of these properties are also presented,
 340 respectively. A regression analysis generates an equation to attempts to explain the statistical
 341 relationship between one or more predictors and the response variable.

342

$$FE = -314.084 + 113.851 \cdot \%F + 70.6381 \cdot FL + 384.347 \cdot Cr - 19.6163 \cdot \%F \cdot FL - 155.064 \cdot \%F \cdot Cr - 70.4887 \cdot FL \cdot Cr + 22.2370 \cdot \%F \cdot FL \cdot Cr \quad (R^2 = 99.02\%); \quad FE = [16.68; 391.23] \quad (8)$$

$$RWP = -21.7027 + 4.75874 \cdot \%F + 4.01494 \cdot FL + 25.4552 \cdot Cr - 0.686908 \cdot \%F \cdot FL - 7.11968 \cdot \%F \cdot Cr - 4.27127 \cdot FL \cdot Cr + 0.946910 \cdot \%F \cdot FL \cdot Cr \quad (R^2 = 98.21\%); \quad RWP = [0.33; 19.23] \quad (9)$$

343

344 The outliers were excluded from the set of results, and the terms considered non-significant by
 345 ANOVA of the regression models were underlined.

346 FE is the energy per unit area needed to completely fracture the composite in quasi stable crack
 347 propagation process in order to record the contribution of all toughness mechanisms mainly
 348 promoted by the fibers. The RWP is the ratio of the plastic working and the elastic work i. e.
 349 indicates the degree of pseudoplastic deformation, that is, it shows that capability of the cement
 350 composite to absorb energy.

351 The ECC reinforced with 2% of fibers presented a significant statistical FE value in relation to ECC
 352 with 1% at 7d and after accelerated aging (200C), based on Equation 8 and Figure 7a. According to
 353 Rodrigues and Montardo [36] and Bentur and Mindess [37], the fiber content provides greater post-
 354 cracking energy and smaller size of the cracks, since the fibers help to absorb the elastic energy
 355 necessary to propagate cracks, which occur between fiber fractions. Regarding the fiber length, the
 356 average value of FE of the composite with fiber of 10 mm is higher than one with fibers of 6 mm,
 357 according to the ANOVA, as calculated by Equation 9 and demonstrated in Figure 7b, before
 358 accelerated aged. However, FE values of composites with fibers of 10 mm presented major standard
 359 deviations than ones with fibers of 6 mm. Fiber with length of 6 mm has a higher number of
 360 filaments per mass, but fiber of 10 mm presented more efficiency in relation to pullout mechanism
 361 that increased average values of the FE and RWP. Fiber with 10 mm has a better degree of adhesion
 362 in the cementitious matrix between the different lengths of fibers, i.e. there is a greater probability
 363 of shorter fibers be pulled without an effective frictional energy. For a surface shear stress applied

364 to the fiber, this will be more efficient if its length is capable of allowing the shear stress permits the
 365 development of a tensile stress equal to its tensile strength [37,38]. From the individual statistical
 366 factors, increases in fiber content and length promote increases in FE and RWP values and the best
 367 type of cure is 7d, however, the interaction between the three statistical factors (fiber fractions (%
 368 F) [1, 2%], fiber length (FL) [6, 10 mm] and curing type (Cr) [7d, 200C]), the highest value for FE
 369 and RWP occurs from the combination with 2% of fibers, 10 mm in length and after 200C.
 370

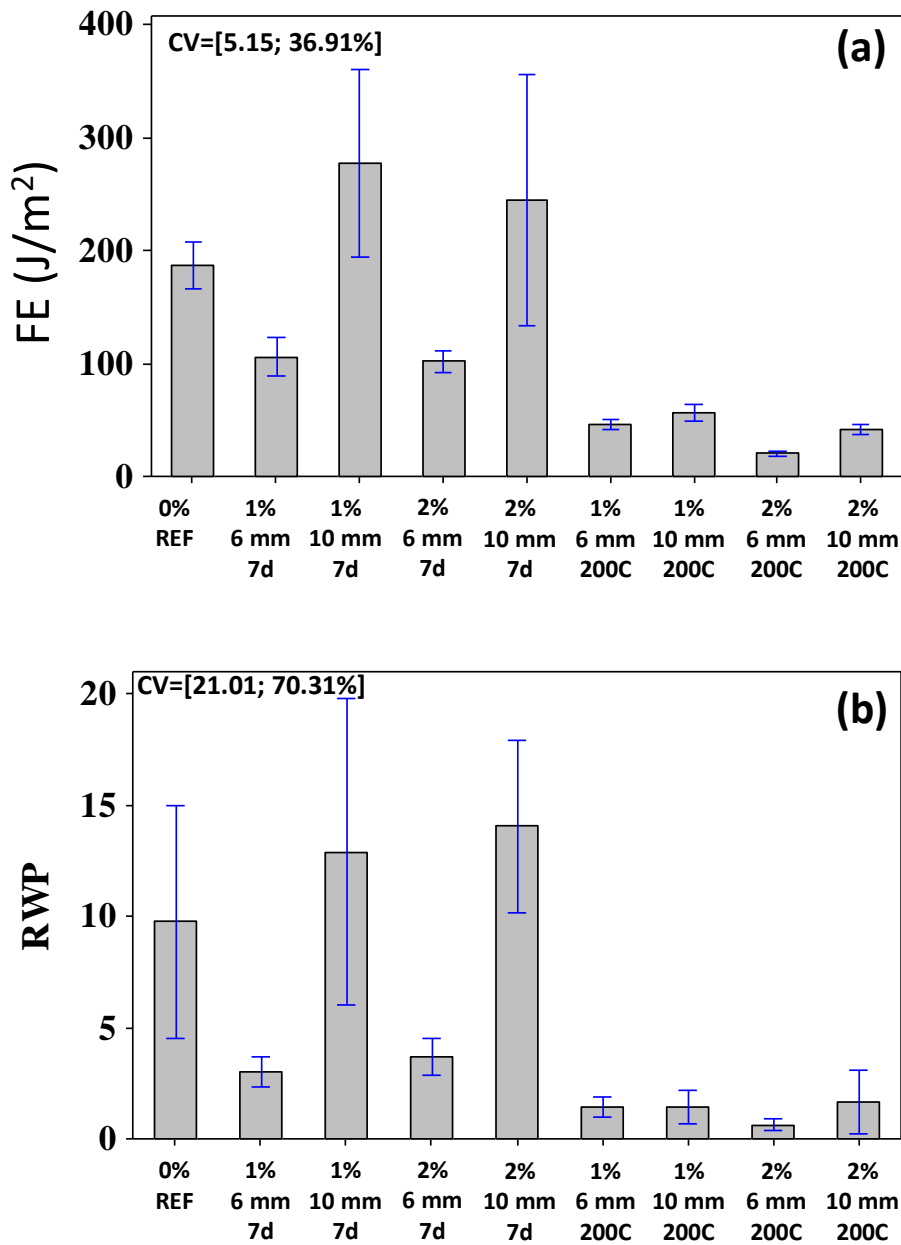
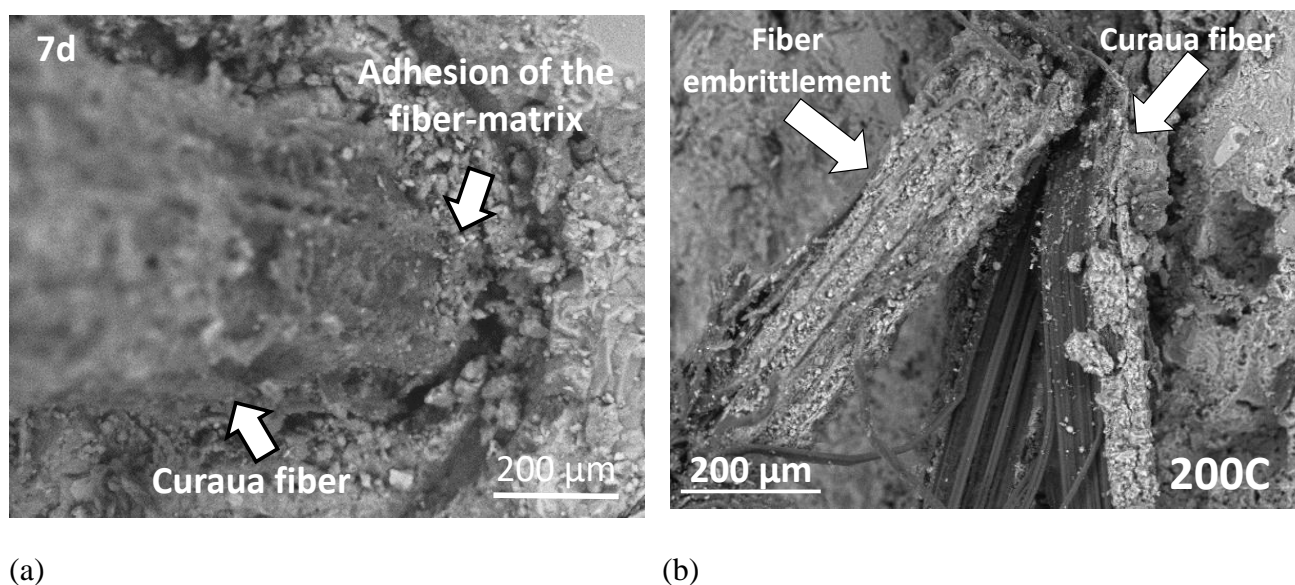


Figure 7 – Average values and standard deviation (FE) Fracture energy (a) and (RWP) relative work of crack propagation (b) in the composite extruded.

372 ECC reinforced with 1% / 10 mm length presented the highest average FE value of 310 J/m² and
373 57 J/m², at 7d and after 200C, respectively. The value of FE at 7d was higher than one determined
374 by Santos et al. (2015), which produced extruded composite reinforced with 2% by mass of
375 eucalyptus cellulosic pulp and 3% by mass of sisal fibers with a length distribution between 1 mm
376 and 14 mm, 7 days cure and exposed to supercritical carbonation. It presented average value of FE
377 approximately 230 J/m². Correia et al., [39] worked with extruded composites reinforced with
378 hybrid cellulosic fibers (8% cellulosic fibers + 1% bamboo nanofibers) that presented FE value
379 around 430 J/m² at 28 days of cure, but it decreased for 271 J/m² after accelerated aging of 200C.
380 The reduction of the FE value after accelerated aging indicates that degradation of the fibers in the
381 ECC caused debonding and breakage of fibers as illustrated in Figures 8a and 8b.
382



(a) (b)
Figure 8 - SEM micrographs of composite extruded at 7d (a) the arrow shows deboning fiber from cement matrix after 200 cycles (b) broken fiber

383

384 **3.2. Physical Characterization**

385 In Figure 9 are shown the graphs with the average values of the physical parameters: water
386 absorption (WA), bulk density (BD) and apparent porosity (AP) of the composites at 7 days and
387 after 200C between level fiber fraction and lengths of curauá fiber (CF). The confidence intervals of
388 the mean (at the 95% confidence level) and the range of variation of the coefficient of variation
389 (CV). The P-values of the Anderson-Darling normality test of the ANOVA residues for the three
390 physical properties (WA, BD and AP) evaluated ranged from 0.109 to 0.918, validating the
391 ANOVA model. Although the coefficient of determination obtained for the estimation of apparent
392 porosity (AP) was 33.22%, all regression models were considered significant by ANOVA.

393 Equations 10, 11 and 12 expresses the regression analysis obtained in the estimation of the WA, BD
 394 and AP values, and also the coefficients of determination (R^2) and the numerical intervals of this
 395 property are presented, respectively.

396

$$WA=10.0648+5.32864 \cdot \%F+0.743583 \cdot \underline{FL}+3.14206 \cdot \underline{Cr}-0.560438 \cdot \%F \cdot \underline{FL}-2.83893 \cdot \%F \cdot \underline{Cr}-0.341080 \cdot \underline{FL} \cdot \underline{Cr}+0.329509 \cdot \%F \cdot \underline{FL} \cdot \underline{Cr} \quad (R^2=92.09\%); \quad WA = [16.24; 18.47] \quad (10)$$

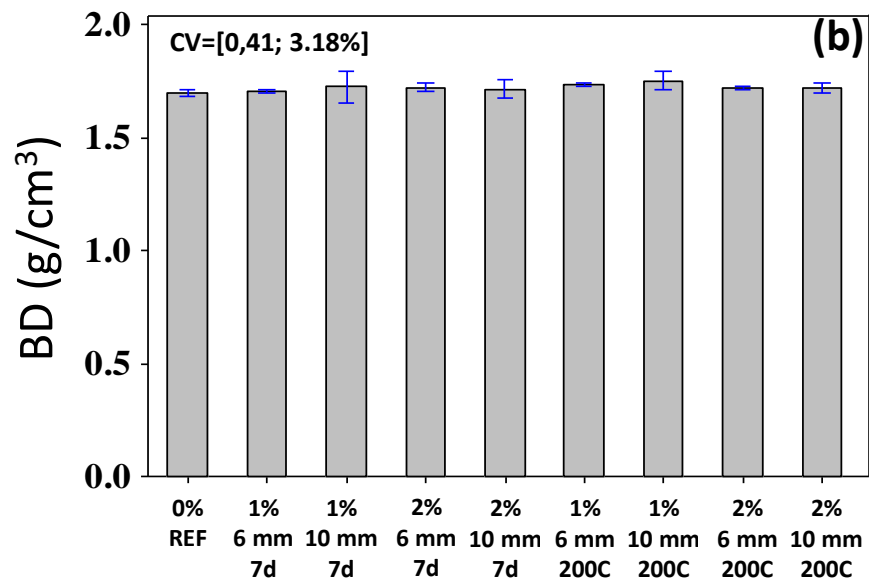
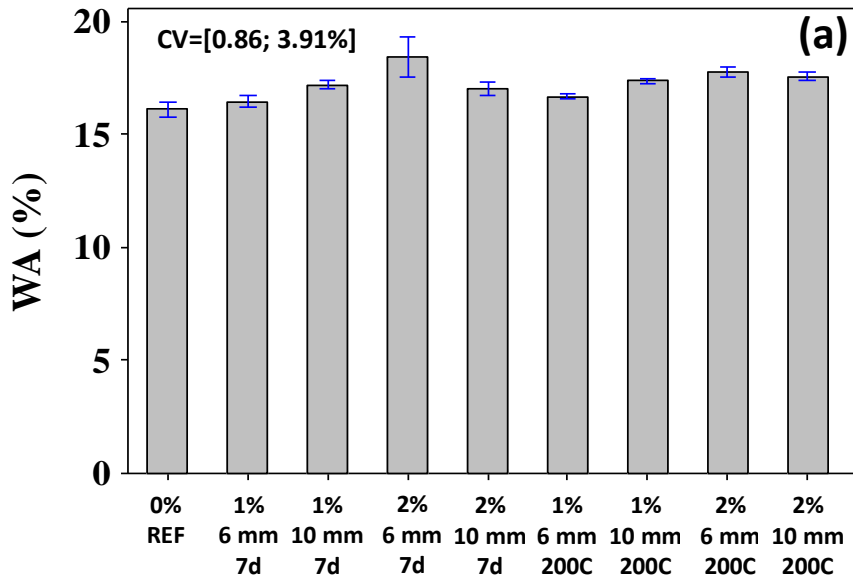
$$BD=17.5215+8.65426 \cdot \%F+1.21420 \cdot \underline{FL}+5.76981 \cdot \underline{Cr}-0.883184 \cdot \%F \cdot \underline{FL}-4.71053 \cdot \%F \cdot \underline{Cr}-0.506878 \cdot \underline{FL} \cdot \underline{Cr}+0.486204 \cdot \%F \cdot \underline{FL} \cdot \underline{Cr} \quad (R^2=84.44\%); \quad BD = [27.86; 31.98] \quad (11)$$

$$AP=1.61519+0.0700806 \cdot \%F+0.0122749 \cdot \underline{FL}+0.160396 \cdot \underline{Cr}-0.00855097 \cdot \%F \cdot \underline{FL}-0.0935377 \cdot \%F \cdot \underline{Cr}-0.0158791 \cdot \underline{FL} \cdot \underline{Cr}+0.0100770 \cdot \%F \cdot \underline{FL} \cdot \underline{Cr} \quad (R^2=33.22\%); \quad AP = [1.67; 1.82] \quad (12)$$

397 Equations 10 to 12, the outliers were excluded from the set of results, and the terms considered non-
 398 significant by ANOVA of the regression analysis were underlined.

399 ECC reinforced with 2% of curauá fiber (CF) presented higher values of WA in relation to the
 400 formulation with 1% by mass showed in Equation 10 and Figure 9a, possibly due to the greater
 401 number of fibers per unit volume conducting to inefficient packaging of the matrix, aspect ratios of
 402 the fibers, CF (80 and 133, respectively for lengths of 6 mm and 10 mm) and, consequently more
 403 defects appears in the interface fiber and matrix [40,41]. The results of fiber length and type of cure
 404 did not differ significantly between the formulations according the ANOVA. The interaction
 405 between the three statistical factors (fiber fractions (% F) [1, 2%], fiber length (FL) [6, 10 mm] and
 406 curing type (Cr) [7d, 200C]), the highest value occurs from the combination with 2% of fibers, 6
 407 mm or 10 mm in length at 7d or after 200C.

408 Composites with 2% by mass of fibers after 200C presented an increase significant of the BD
 409 values showed in Equation 11 and Figure 9b, which can be attributed the filling of the matrix pores
 410 by the continued hydration process during accelerated aging cycles in formation of calcium
 411 hydroxide ($Ca(OH)_2$), calcium silicate hydrate (CSH) and calcium carbonate ($CaCO_3$) [13]. These
 412 phenomena were found in several studies that have been applied accelerated aging cycles in
 413 composites cementitious, such as Soto et al., [35]; Dias et al., [42] and Teixeira [4]. The only
 414 individual factor statistical that did not affect the bulk density (BD) values was the fiber length.
 415 Thus, the interaction between the three statistical factors (fiber fractions (% F) [1, 2%], fiber length
 416 (FL) [6, 10 mm] and curing type (Cr) [7d, 200C]), the highest value occurs from the combination
 417 with 2% of fibers, 6 mm or 10 mm in length and after 200C.



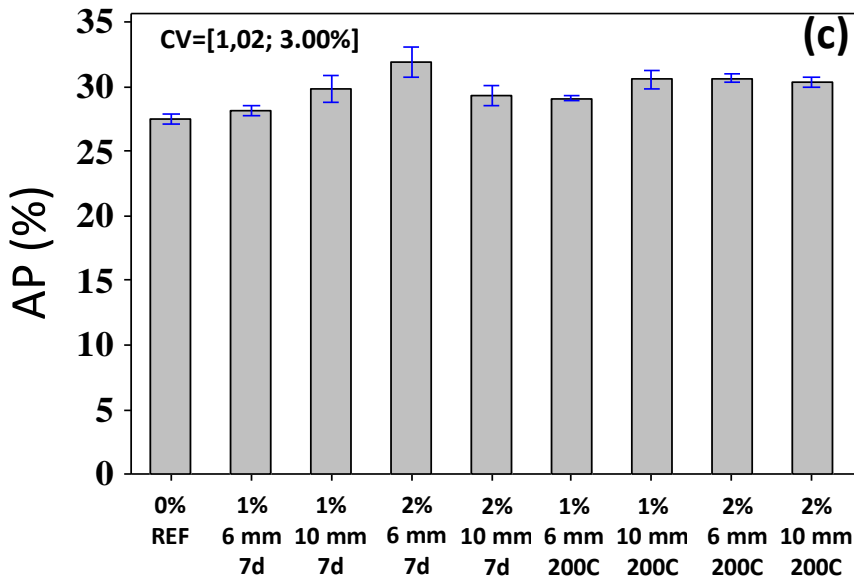


Figure 9 - Results of the physical properties: (WA) water absorption (a); (BD) bulk density (b) and (AP) Apparent porosity (c).

418

419 According to the ANOVA, considering the individual statistical factors and the interaction, only the
 420 accelerated aging (200C) promoted significant differences in the values of the apparent porosity
 421 (AP) of the composites shown in Equation 12 and Figure 9c. It is believed that the immersion and
 422 drying cycles caused higher incidence of pores as result of microcracks caused by the aging cycles
 423 [39]. At the initial period of the immersion cycles, lignocellulosic fiber could absorb the water from
 424 the cementitious microstructure since the surrounding water concentration is greater than within the
 425 fibers. At a later stage of drying cycles, the moisture content within the fibers dry out and thus,
 426 fibers shrink to a smaller size. The shrinkage of the fiber generates microcracks between the fiber
 427 and cement matrix, creating voids that explain the low results of FE and RWP in the transition zone
 428 [29,39]. From the interaction between the three statistical factors (fiber fractions (% F) [1, 2%],
 429 fiber length (FL) [6, 10 mm] and curing type (Cr) [7d, 200C]), the highest value occurs from the
 430 combination with 1% or 2% of fibers, 6 mm or 10 mm in length at 7d.

431

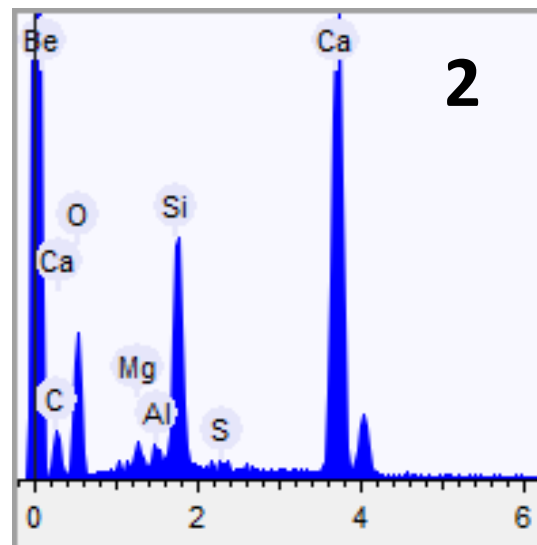
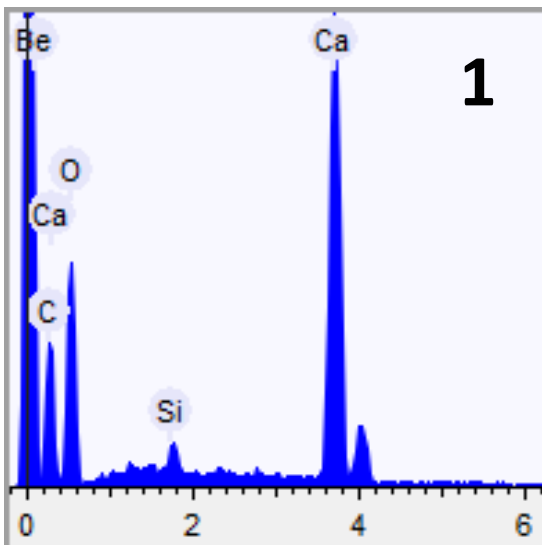
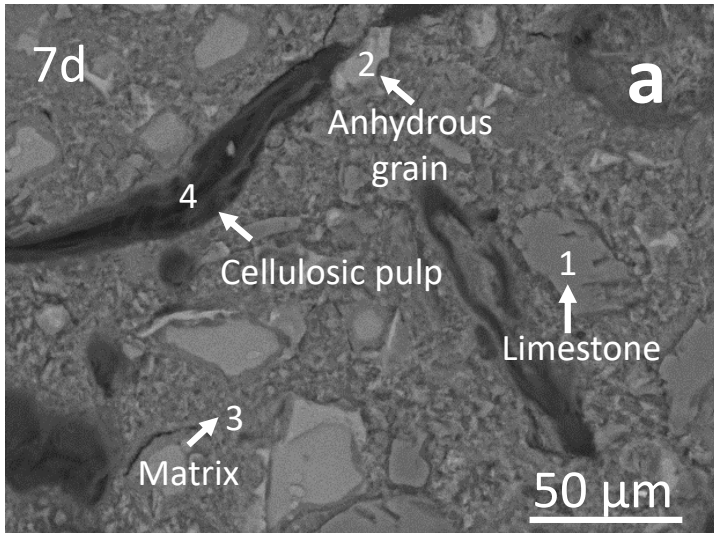
432 3.3. Micrographic electronic scanning SEM

433 Figure 10 shows the micrographs (SEM) with EDS in the composites reinforced with CF detaching
 434 the points of chemical elements in cementitious structures. The dark areas in the image (associated
 435 with low atomic number of the predominant chemical elements) correspond to the longitudinal
 436 sections of the fibers.

437 In point 1, identifies the grain with a high calcium index from the formulation used about 27% of

438 limestone in the mix. In point 2, detaching the anhydrous grain that was not completely hydrated,
439 predominantly Si and Ca elements.

440 Point 3 clearly shows a grain formed cement constituents. In point 4, the cellulose pulp with a high
441 calcium content and silicon are shown, indicating that the fiber absorbed cement hydration water,
442 which was similar to that presented by Tonoli et al., [43] and Teixeira et al., [29], who studied
443 eucalyptus cellulosic pulp.
444



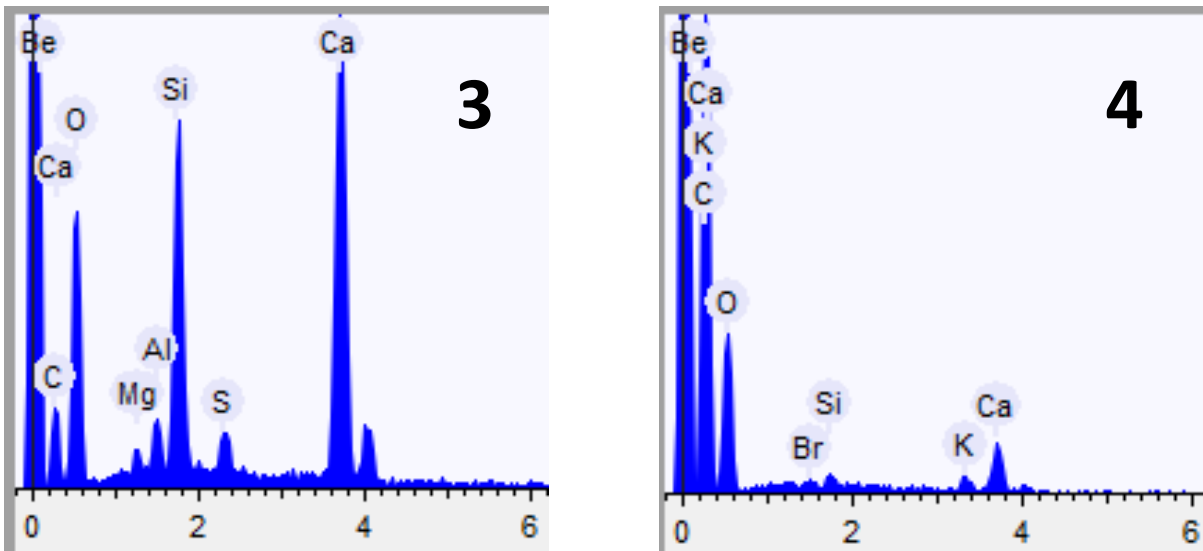


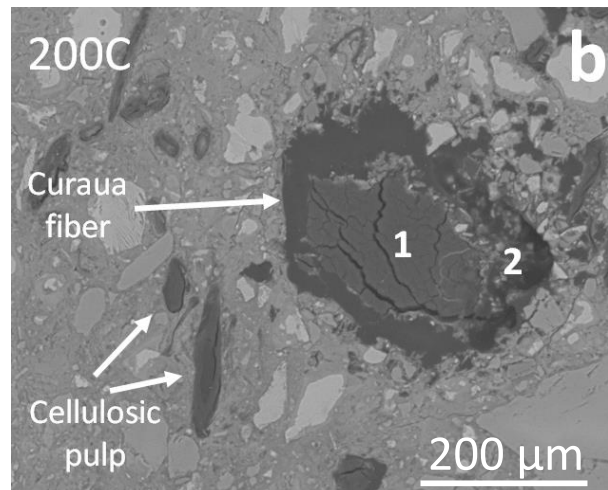
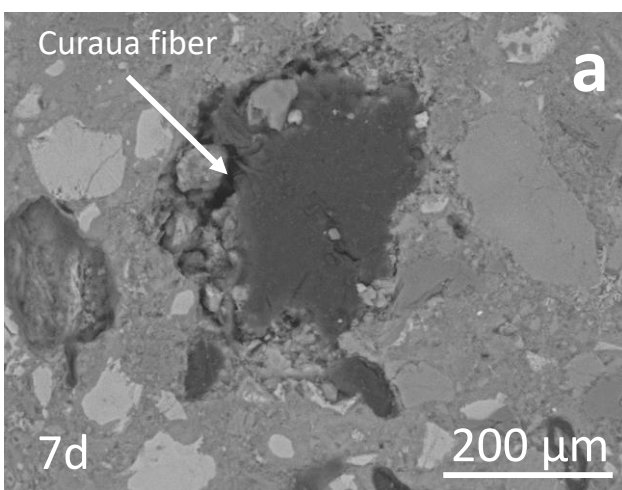
Figure 10 – (a) Image Scanning electron microscopy (SEM-BSE) polished surfaces of composites reinforced with CF and points of EDS analyzes that are marked on the images (1 to 4): (1) limestone; (2) anhydrous grain; (3) cementitious matrix and (4) cellulosic pulp

445

446 In Figure 11a, it is observed a resulted of the dimensional variation of fiber according to its
 447 humidity content. Resulting pores lead to higher water absorption, greater porosity and low
 448 resistance.

449 Savastano and Agopyan [44], explain that the best performance is achieved by better adhesion of
 450 the fiber-matrix. The improved adherence is achieved by reducing the porosity and the lowest
 451 concentration of Portlandite (calcium hydroxide crystals) approximately the fiber.

452



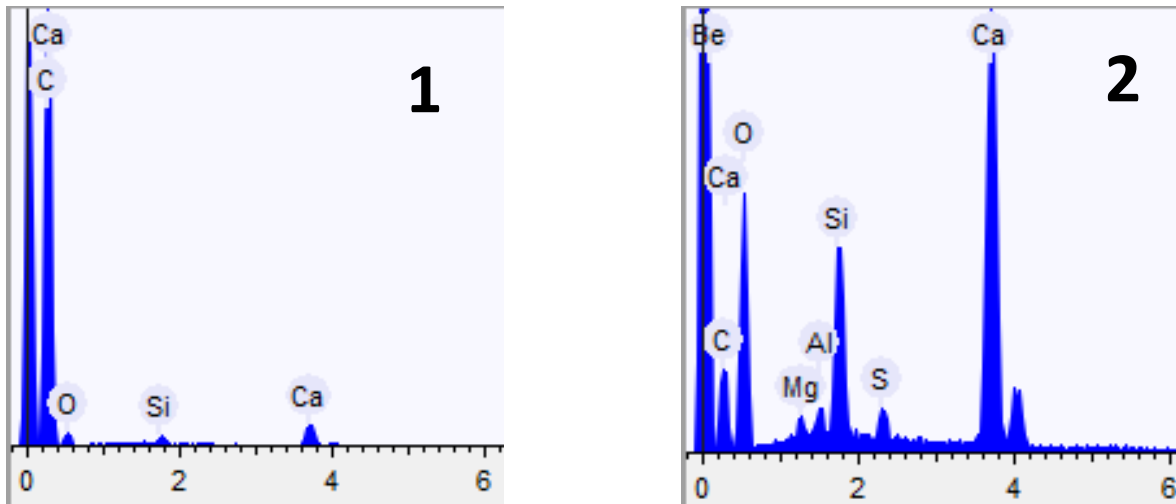


Figure 11 – Micrograph of scanning electron microscopy (SEM-BSE) polished surfaces of composites reinforced with CF: (a) CF (arrow indicates adhesion fiber-cement) and (b) CF after 200C with points of EDS analysis that is signaled the image (point 1 and 2).

453

454 In Figure 11b, after 200 cycles, there is better adhesion of the fiber in the matrix. Point 1 shows that,
 455 in the central part of the fiber were not found cement hydration products as indicated by the EDS, the
 456 large presence of C. However, at point 2, the border of the fiber presents the main chemical elements
 457 of cement, silicon and calcium [19,45].

458 They can also be observed by EDS, chemical elements, such as, Al, S, and Mg. This phenomenon can
 459 be associated with mineralization fibers as indicated by Bentur and Akers [46]. On immersion in
 460 water, free ions formed by the dissolution of the cementitious phases of Portland cement penetrated
 461 into the lumen of the fibers, leading to the formation of ettringite/monosulfates and calcium hydroxide
 462 Ca(OH) [29,45]. Batic et al., [47] showed that the re-precipitation of ettringite in microcracks and
 463 pores of the cementitious composite may occur under normal conditions (ambient temperature)
 464 curing. Such training has previously been suggested as one of the degradation mechanisms of the
 465 fibers within the concrete matrix [14,15].

466

467 4. CONCLUSIONS

468 The curauá fiber suffered mineralization process during curing (water absorption of the cement
 469 hydration products) which consequently carried the fiber to decreased its properties. The fiber
 470 content directly influenced the mechanical performance and fibers with lengths greater showed
 471 better mechanical results for modulus of rupture (MOR) and fracture energy (FE) according to
 472 ANOVA. Cementitious composites reinforced with fibers curauá showed superior mechanical
 473 performance compared to available research literature. The modulus of rupture (MOR), fracture
 474 energy (FE) and relative working crack propagation (RWP) results of the composites reinforced

475 with fibers curauá after 200 accelerated aging cycles were better in relation of the composites at 7
476 days, because of the cement hydration, which filled the pores, densified its structure, which
477 improved the transition zone fiber matrix. On the other hand, the aging promoted mineralization of
478 the fiber, which reduced the mechanical performance of composites with curauá compared with
479 literature researches. Thus, the best results were obtained for composites reinforced with 2% of
480 curauá fiber with 10 mm of length after 200C.

481 In the physical results, the composite with 2% of fiber increased by water absorption and bulk
482 density due to the greater number of fibers per unit volume and the filling of the matrix pores by the
483 continued hydration process during accelerated aging cycles (200C) in formation of calcium
484 hydroxide ($\text{Ca}(\text{OH})_2$), calcium silicate hydrate (CSH) and calcium carbonate (CaCO_3) respectively.
485 Considering the individual statistical factors and the interaction, only the accelerated aging (200C)
486 promoted significant differences in the values of the apparent porosity (AP). It is believed that the
487 immersion and drying cycles caused higher incidence of pores as result of microcracks caused by
488 the aging cycles. According to the ANOVA, the only individual factor statistical that did not affect
489 the physical values was the fiber length. Thus, the interaction between the three statistical factors,
490 the highest value occurs from the combination with 2% of curauá fibers, 6 mm or 10 mm in length
491 after 200C.

492 Scanning electron microscopy of the fracture surface of curauá fibers showed chemical elements
493 from the cement inside the fiber. Also showed detachment of the fibers from the cement matrix
494 indicating low mechanical performance.

495 These results encourage us to use composites reinforced with curauá fiber in constructions in indoor
496 environments as ceiling and partitions. New tests should be used to optimize results.

497

498 **5. ACKNOWLEDGEMENTS**

499 The authors acknowledge the financial support provided by Brazilian Agencies: Fundação de
500 Amparo à Pesquisa do Estado de São Paulo (FAPESP, Grant nº 2013/03823-8 and 2012/51467-3);
501 Coordenação de Aperfeiçoamento de Pessoal de Nível Superior (CAPES, Grant nº 3886/2014); and
502 Conselho Nacional de Desenvolvimento Científico e Tecnológico (CNPq, Grant nº 406429/2015
503 and 312151/2016-0). The authors thank the Brazilian companies Fibria S.A., Infibra S.A. and
504 Imbralit Ltda. for technical support to the development of this work.

505

506 **6. REFERENCE**

507 [1] S.F. Santos, J.D.A. Rodrigues, G.H.D. Tonoli, A.E.F.D.S. Almeida, H. Savastano Jr, Effect

- 508 of colloidal silica on the mechanical properties of fiber–cement reinforced with cellulosic
509 fibers, *J. Mater. Sci.* 49 (2014) 7497–7506. doi:10.1007/s10853-014-8455-1.
- 510 [2] S. Ikai, J.R. Reichert, A. V. Rodrigues, V.A. Zampieri, Asbestos-free technology with new
511 high toughness polypropylene (PP) fibers in air-cured Hatschek process, *Constr. Build.*
512 *Mater.* 24 (2010) 171–180. doi:10.1016/j.conbuildmat.2009.06.019.
- 513 [3] F. Pacheco-Torgal, S. Jalali, Cementitious building materials reinforced with vegetable
514 fibres: A review, *Constr. Build. Mater.* 25 (2011) 575–581.
515 doi:10.1016/j.conbuildmat.2010.07.024.
- 516 [4] R.S. Teixeira, G.H.D. Tonoli, S.F. Santos, J. Fiorelli, H. Savastano Jr., F.A.R. Lahr,
517 Extruded Cement Based Composites Reinforced with Sugar Cane Bagasse Fibres, *Key Eng.*
518 *Mater.* 517 (2012) 450–457. doi:10.4028/www.scientific.net/KEM.517.450.
- 519 [5] T. Tan, S.F. Santos, H. Savastano Jr, W.O. Soboyejo, Fracture and resistance-curve behavior
520 in hybrid natural fiber and polypropylene fiber reinforced composites, *J. Mater. Sci.* 47
521 (2012) 2864–2874. doi:10.1007/s10853-011-6116-1.
- 522 [6] C.S. Fonseca, T.F. Silva, M.F. Silva, I.R.C. Oliviera, R.F. Mendes, P.R.G. Hein, L.M.
523 Mendes, G.H.D. Tonoli, Micro/Nanofibrilas celulósicas de eucalyptus em fibrocimentos
524 extrudados, *Cerne.* 22 (2016) 59–68. doi:10.1590/01047760201622012084.
- 525 [7] C.R. Araújo, L.C. Perlaza, C.G. Mothé, Thermal properties of commercial and castor oil
526 polyurethane composites with curauá fiber, in: *Fourth Int. Symp. Nat. Polym. Compos.* 2002,
527 São Paulo, 2002.
- 528 [8] F. Tomczak, K.G. Satyanarayana, T.H.D. Sydenstricker, Studies on lignocellulosic fibers of
529 Brazil: Part III - Morphology and properties of Brazilian curauá fibers, *Compos. Part A Appl.*
530 *Sci. Manuf.* 38 (2007) 2227–2236. doi:10.1016/j.compositesa.2007.06.005.
- 531 [9] M.A.S. Spinacé, C.S. Lambert, K.K.G. Feroselli, M.A. De Paoli, Characterization of
532 lignocellulosic curaua fibres, *Carbohydr. Polym.* 77 (2009) 47–53.
533 doi:10.1016/j.carbpol.2008.12.005.
- 534 [10] D.G. Soltan, P. das Neves, A. Olvera, H. Savastano Jr, V.C. Li, Introducing a curauá fiber
535 reinforced cement-based composite with strain-hardening behavior, *Ind. Crops Prod.* 103
536 (2017) 1–12. doi:10.1016/j.indcrop.2017.03.016.
- 537 [11] K.G. Kuder, S.P. Shah, Processing of high-performance fiber-reinforced cement-based
538 composites, *Constr. Build. Mater.* 24 (2010) 181–186.
539 doi:10.1016/j.conbuildmat.2007.06.018.
- 540 [12] C. Aldea, S. Marikunte, S.P. Shah, Extruded fiber reinforced cement pressure pipe, *Adv.*
541 *Cem. Based Mater.* 8 (1998) 47–55. doi:10.1016/S1065-7355(98)00006-6.
- 542 [13] S.F. Santos, R. Schmidt, A.E.F.S. Almeida, G.H.D. Tonoli, H. Savastano Jr, Supercritical
543 carbonation treatment on extruded fibre–cement reinforced with vegetable fibres, *Cem.*
544 *Concr. Compos.* 56 (2015) 84–94. doi:10.1016/j.cemconcomp.2014.11.007.
- 545 [14] B.J. Mohr, H. Nanko, K.E. Kurtis, Durability of kraft pulp fiber – cement composites to
546 wet/dry cycling, *Cem. Concr. Compos.* 27 (2005) 435–448.
547 doi:10.1016/j.cemconcomp.2004.07.006.
- 548 [15] B.J. Mohr, J.J. Biernacki, K.E. Kurtis, Microstructural and chemical effects of wet/dry
549 cycling on pulp fiber-cement composites, *Cem. Concr. Res.* 36 (2006) 1240–1251.
550 doi:10.1016/j.cemconres.2006.03.020.

- 551 [16] G.H.D. Tonoli, M.N. Belgacem, G. Siqueira, J. Bras, H. Savastano Jr, F.A. Rocco Lahr,
552 Processing and dimensional changes of cement based composites reinforced with surface-
553 treated cellulose fibres, *Cem. Concr. Compos.* 37 (2013) 68–75.
554 doi:10.1016/j.cemconcomp.2012.12.004.
- 555 [17] J. de A. Melo Filho, F. de A. Silva, R.D. Toledo Filho, Degradation kinetics and aging
556 mechanisms on sisal fiber cement composite systems, *Cem. Concr. Compos.* 40 (2013) 30–
557 39. doi:10.1016/j.cemconcomp.2013.04.003.
- 558 [18] A.E.F.S. Almeida, G.H.D. Tonoli, S.F. Santos, H. Savastano Jr, Improved durability of
559 vegetable fiber reinforced cement composite subject to accelerated carbonation at early age,
560 *Cem. Concr. Compos.* 42 (2013) 49–58. doi:10.1016/j.cemconcomp.2013.05.001.
- 561 [19] R.S. Teixeira, G.H.D. Tonoli, S.F. Santos, H. Savastano Jr, T.P. Protásio, E.F. Toro, J.
562 Maldonado, F.A.R. Lahr, S. Delvasto, Different ageing conditions on cementitious roofing
563 tiles reinforced with alternative vegetable and synthetic fibres, *Mater. Struct.* 47 (2014) 433–
564 446. doi:10.1617/s11527-013-0070-0.
- 565 [20] L.K. Aggarwal, Bagasse-reinforced cement composites, *Cem. Concr. Compos.* 17 (1995)
566 107–112.
- 567 [21] TAPPI T 204 cm-97, Solvent extractives of wood and pulp, TAPPI TEST METHODS. Tech.
568 Assoc. Pulp an Pap. Ind. Atlanta, GA. Tappi Press. (1997) 1–4.
- 569 [22] T. Zimmermann, N. Bordeanu, E. Strub, Properties of nanofibrillated cellulose from different
570 raw materials and its reinforcement potential, *Carbohydr. Polym.* 79 (2010) 1086–1093.
571 doi:10.1016/j.carbpol.2009.10.045.
- 572 [23] TAPPI T 222 om-02, Acid-insoluble lignin in wood and pulp, TAPPI TEST METHODS.
573 Tech. Assoc. Pulp an Pap. Ind. Atlanta, GA. Tappi Press. (2002) 1–5.
- 574 [24] O. Faruk, A.K. Bledzki, H.-P. Fink, M. Sain, Progress Report on Natural Fiber Reinforced
575 Composites, *Macromol. Mater. Eng.* 299 (2014) 9–26. doi:10.1002/mame.201300008.
- 576 [25] J.C. Caraschi, A.L. Leão, Characterization of Curaua Fiber, *Mol. Cryst. Liq. Cryst. Sci.*
577 *Technol. Sect. A. Mol. Cryst. Liq. Cryst.* 353 (2000) 149–152.
578 doi:10.1080/10587250008025655.
- 579 [26] S.F. Santos, R.S. Teixeira, H. Savastano Jr., Interfacial transition zone between
580 lignocellulosic fiber and matrix in cement-based composites, in: *Sustain. Nonconv. Constr.*
581 *Mater. Using Inorg. Bond. Fiber Compos.*, 6, Woodhead Publishing, 2017: pp. 27–68.
- 582 [27] ASTM C 150, Am. Soc. Test. Mater. – ASTM C150/C150M-11. *Stand. Specif. Portl. Cem.*
583 (2011).
- 584 [28] F.A. Cardoso, R.G. Pileggi, V.M. John, Caracterização reológica de argamassas pelo método
585 de squeeze flow, in: *VI Simpósio Bras. Tecnol. Argamassa, 2005*, p. 121-143, Florianópolis,
586 2005: pp. 121–143.
- 587 [29] R.S. Teixeira, G.H.D. Tonoli, S.F. Santos, E. Rayón, V. Amigó, H. Savastano Jr, F.A. Rocco
588 Lahr, Nanoindentation study of the interfacial zone between cellulose fiber and cement
589 matrix in extruded composites, *Cem. Concr. Compos.* 85 (2018) 1–8.
590 doi:10.1016/j.cemconcomp.2017.09.018.
- 591 [30] J. Nakayama, Direct Measurement of Fracture Energies of Brittle Heterogeneous Materials,
592 *J. Am. Ceram. Soc.* 48 (1965) 583–587. doi:10.1111/j.1151-2916.1965.tb14677.x.
- 593 [31] S. Ribeiro, J.A. Rodrigues, The influence of microstructure on the maximum load and

- 594 fracture energy of refractory castables, *Ceram. Int.* 36 (2010) 263–274.
595 doi:10.1016/j.ceramint.2009.07.033.
- 596 [32] ASTM C 948-81, Am. Soc. Test. Mater. ASTM C 948-82 Test Method Dry Wet Bulk
597 Density, Water Absorption, Apparent Porosity Thin Sect. Glas. Reinf. Concr. West
598 Conshohocken, PA, USA. 1982. (1982).
- 599 [33] EN 494, Eur. Comm. Stand. EN 494 Fibre-Cement Profiled Sheets Fitt. Roof. – Prod. Specif.
600 Test Methods. London, UK. BSI – Br. Stand. Institution. 1994. (1994).
- 601 [34] A. Bentur, S.A.S. Akers, The microstructure and ageing of cellulose fibre reinforced
602 autoclaved cement composites, *Int. J. Cem. Compos. Light. Concr.* 11 (1989) 111–115.
603 doi:10.1016/0262-5075(89)90121-8.
- 604 [35] Y.J.M. Soto, G.H.D. Tonoli, R.S. Teixeira, S.F. Santos, H. Savastano Jr, Prospective study
605 on vegetable wastes as reinforcement in extruded fibre-cement., in: *Int. Conf. Non-
606 Conventional Mater. Technol. Ecol. Mater. Technol. Sustain. Constr. 2007.*, Anais do Brasil-
607 NOCMAT. (Abmtenc), Maceió, 2007.
- 608 [36] P.P.F. Rodrigues, J.P.A. Montardo, Influência da adição de fibras de polipropileno nas
609 propriedades dos concretos para pisos e pavimentos., in: *44º Congr. Bras. Do Concreto,
610 2002*, Instituto Brasileiro do Concreto – IBRACON, Belo Horizonte, 2002.
- 611 [37] A. Bentur, S. Mindess, *Fibre reinforced cementitious composites*, Elsevier Applied Science,
612 449 p, England, 1990.
- 613 [38] H.F.W. Taylor, *Cement chemistry*, Academic press limited, 475p, London, 1990.
- 614 [39] V. da C. Correia, S.F. Santos, R.S. Teixeira, H. Savastano Jr, Nanofibrillated cellulose and
615 cellulosic pulp for reinforcement of the extruded cement based materials, *Constr. Build.
616 Mater.* 160 (2018) 376–384. doi:10.1016/j.conbuildmat.2017.11.066.
- 617 [40] E.M. Bezerra, A.P. Joaquim, H. Savastano Jr, V.M. John, V. Agopyan, The effect of
618 different mineral additions and synthetic fiber contents on properties of cement based
619 composites, *Cem. Concr. Compos.* 28 (2006) 555–563.
620 doi:10.1016/j.cemconcomp.2006.02.001.
- 621 [41] G.H.D. Tonoli, H. Savastano Jr, S.F. Santos, C.M.R. Dias, V.M. John, F.A.R. Lahr, Hybrid
622 reinforcement of sisal and polypropylene fibers in cement-based composites, *J. Mater. Civ.
623 Eng.* 23 (2011) 177–187. doi:10.1061/(ASCE)MT.1943-5533.0000152.
- 624 [42] C.M.R. Dias, H. Savastano Jr., V.M. John, Exploring the potential of functionally graded
625 materials concept for the development of fiber cement, *Constr. Build. Mater.* 24 (2010) 140–
626 146. doi:10.1016/j.conbuildmat.2008.01.017.
- 627 [43] G.H.D. Tonoli, U.P. Rodrigues Filho, H. Savastano Jr, J. Bras, M.N. Belgacem, F.A. Rocco
628 Lahr, Cellulose modified fibres in cement based composites, *Compos. Part A Appl. Sci.
629 Manuf.* 40 (2009) 2046–2053. doi:10.1016/j.compositesa.2009.09.016.
- 630 [44] H. Savastano Jr, V. Agopyan, Transition zone studies of vegetable fibre-cement paste
631 composites, *Cem. Concr. Compos.* 21 (1999) 49–57. doi:10.1016/S0958-9465(98)00038-9.
- 632 [45] R. MacVicar, L.M. Matuana, J.J. Balatinecz, Aging mechanisms in cellulose fiber reinforced
633 cement composites, *Cem. Concr. Compos.* 21 (1999) 189–196. doi:10.1016/S0958-
634 9465(98)00050-X.
- 635 [46] A. Bentur, S.A.S. Akers, The microstructure and ageing of cellulose fibre reinforced cement
636 composites cured in a normal environment, *Int. J. Cem. Compos. Light. Concr.* 11 (1989)

637 99–109. doi:10.1016/0262-5075(89)90120-6.

638 [47] O.R. Batic, C.A. Milanesi, P.J. Maiza, S.A. Marfil, Secondary ettringite formation in
639 concrete subjected to different curing conditions, *Cem. Concr. Res.* 30 (2000) 1407–1412.
640 doi:10.1016/S0008-8846(00)00343-4.

641